Automatic Parameter Estimation for Graph-Cut Chan-Vese for Fluorescence Image Binarization

Ryan Naidoo, Jules-Raymond Tapamo

Abstract

The detailed analytical studies of microscopic organisms and such have played a vital role in a host of fields ranging from the simple curiosity of what goes on at the mirco-level to studying the behaviour of cancerous cells. Fluorescence images are generated by the thousands to study these phenomena. The rate at which we're able to gather data outweighs the rate at which we're able to accurately study it. The purpose of this study is too investigate the properties of fluorescence images and leverage that understanding to develop a technique that is able to automatically produce image-specific accurate parameter settings for segmentation of the object of interest. In this paper, we present a novel parameter estimation technique for the graph cut implementation of the Chan-Vese approximation of the Mumford-Shah functional for image segmentation. The effectiveness of the technique is demonstrated through a set of experiments with real images. We pit our approach against two other common paramter settings. Our segmentation scheme is highly robust and produces superior segmentation results with an average accuracy of 93.533%.

Keywords

Image segmentation, graph cuts, fluorescence, active-contours, Chan-Vese, Mumford-Shah.

I. Introduction

The ability to attain images at levels beyond the capacity of the human eye is an extremely important asset in scientific inquiry and study. Images of the microscopic world inherently contain a lot of useful data which has proven to be immensely helpful in the medical and biological fields [REF HERE]. A common tool for obtaining these images is the fluorescence microscope. The rate at which fluorescent images are generated is capped by the rate at which we're able to effectively and efficiently analyse image data [REF HERE]. At the heart of studying fluorescent images, is the segmentation of the object of interest. Segmentation is almost always the first step in an image analysis pipeline [REF HERE]. Hence, the efficiency of the system as a whole depends strongly on the accuracy of image segmentation. Fluorescence images exhibit a much stronger diversity in comparison to other fields. This poses a problem since it rules out a "golden" parameter setting for any scheme. Many, instead, prefer to work on subdomains within fluorescence imaging and devise a setting for the parameters of a certain scheme [REF HERE]. Though this does help, the scope of the solution is too limited and barely covers all cases within that subdomain. We seek a solution that is able to cover a very broad area with consistently high accuracy and high robustness for all fluorescent images. This means, enabling the parameters to change to suit the image.

In this paper we take a step in that direction by allowing the parameters of the graph cut solution to the Chan-Vese functional to be determined on an image-by-image basis. This is a major step in fluorescent image segmentation. The scheme which we present is readily and easily adaptable to any other field.

The remainder of this paper is organised as follows; firstly, we begin in Section II with a brief introduction to the Chan-Vese formulation of the Mumford-Shah energy functional. Then in Section III we introduce the graph-cut approach to image segmentation and how it is used to solve the Chan-Vese image segmentation problem. We then develop the proposed technique for parameter estimation in Section IV. In Section V we show some experimental results and demonstrate the efficiency and robustness of this scheme. We also compare the proposed scheme against two other well-known schemes. Our concluding remarks are shown in Section VI.

II. Chan-Vese Formulation of the Mumford-Shah Energy Functional

The Mumford-Shah evolution energy functional [REF HERE] is a segmentation model to be minimised over an approximation image u of the input image u_0. The level set representation of the Mumford-Shah energy function is

$$\begin{aligned} F(c_1, c_2, \phi) = \mu &\int_{\Omega} \delta(\phi(x,y))|\nabla\phi(x,y)|dxdy \\ &+ \nu \int_{\Omega} H(\phi(x,y))dxdy \\ &+ \lambda_1 \int_{\Omega} |u(x,y) - c_1|^2 H(\phi(x,y))dxdy \\ &+ \lambda_2 \int_{\Omega} |u(x,y) - c_2|^2 (1 - H(\phi(x,y)))dxdy, \end{aligned} \tag{1}$$

where λ_1, λ_2, μ, and ν are fixed parameters such that $\lambda_1, \lambda_2 > 0$ and $\mu, \nu \geq 0$. $u(x,y)$ is the image, $H(\cdot)$ is the Heaviside step function, $\delta(\cdot)$ is the Dirac delta function, Φ is an open unbounded subset of $\Re^2$ and $\phi : \Omega \to \mathbb{R}$ is the level set function, such that:

$$\begin{aligned} \omega &= \{(x,y) \in \Omega | \Phi(x_p) > 0\} \\ \bar{\omega} &= \{(x,y) \in \Omega | \Phi(x_p) < 0\} \\ C = \partial\omega &= \{(x,y) \in \Omega | \Phi(x_p) = 0\}, \end{aligned} \tag{2}$$

c_1 and c_2 are the arithmetic means of the intensities in the regions of u defined by the masks $H(\phi(x,y))$ and $1 - H(\phi(x,y))$ respectively. The piece-wise smooth approximation of the image is then

$$u(x,y) = c_1 H(\phi(x,y)) + c_2(1 - H(\phi(x,y))). \tag{3}$$

A. Discretising the Mumford-Shah Functional

With the exception of the second term in Equation (1), the remaining terms can be represented discretely very easily. For each pixel $p \in \Omega$, let x_p be a binary variable such that

$$x_p = \begin{cases} 0 & \phi(p) \leq 0 \\ 1 & \phi(p) > 0 \end{cases} \tag{4}$$

The means can now be calculated using

$$c_1 = \frac{\sum_p u(x,y)x_p}{\sum_p x_p}, \tag{5}$$

$$c_2 = \frac{\sum_p u(x,y)(1 - x_p)}{\sum_p (1 - x_p)}. \tag{6}$$

For simplification, set $\nu = 0$. Kolmogorov and Boykov in [REF HERE] used the Cauchy-Crofton thereom to approximate the length of a contour C by counting the number of intersections with the line L. By using this approximation, it can be shown that the Euclidean contour length can be expressed as

$$\|C\|_E = \sum_{p,q \in e_k} w_k(x_p(1-x_q) + x_q(1-x_p)). \tag{7}$$

The fully discrete form of Equation (1) is

$$\begin{aligned} F(x_1, \ldots, x_n) = \mu & \sum_{p,q \in e_k} w_k(x_p(1-x_q) + x_q(1-x_p)) \\ & + \lambda_1 \sum_p |u(x,y) - c_1|^2 x_p \\ & + \lambda_2 \sum_p |u(x,y) - c_2|^2 (1-x_p) \end{aligned} \tag{8}$$

This function is optimised by using the graph cut which we briefly introduce in the next section.

III. Graph-Cut Model for Chan-Vese Segmentation

Graph Cuts are a well known optimisation problem in Combinatronics [REF HERE]. Due to the duality known as the Max-Flow Min-Cut Thereom [REF HERE], there are several fast algorithms to find the mincut. Typically, it's easier to solve the the Max-Flow problem and bulk of the optimised algorithms are designed on Max-flow algorithms. Graph Cuts were unsuccesfully introduce into Computer Vision by Greig *et al.* [REF HERE] and was later popularised by Kolmogorov [REF HERE].

A graph $G = (V, E)$ is a set of vertices/nodes V, and a set of directed edges E with positive weights/capacities that connect these vertices. We let uv be a directed edge going from u to v. The weight of the edge is denoted by $c(u, v)$.

The most common method of representing an image as a graph is to assign a node for each pixel; and connect the neighbouring nodes with an edge. The weight of that edge is generally scaled by some distance metric according to the distance between the nodes. The weight of the edges reflect the correlation between the two corresponding pixels. A typical correlation is the similarity between two neighbouring nodes based on intensity. In the 2-label graph cut, there are two more vertices that don't correspond to any pixels. These are the source s and the sink t. The source node connects to all pixel-nodes, and all pixel-nodes connect to the sink. Therefore, a cut on G is a partioning of V into two disjoint connected sets (V_s, V_t) such that $s \in V_s$ and $t \in V_t$. The cost of the cut is calculated as

$$c(V_s, V_t) = \sum_{i \in V_s, j \in V_t} c(i, j). \tag{9}$$

Graph cuts can be used to minimise energies of the form

$$\arg\min_{x \in \{0,1\}^m} E(x) = \sum_i E^i(x_i) + \sum_{i<j} E^{i,j}(x_i, x_j). \tag{10}$$

The first term is known as the data term and the second term is known as the regularisation/smoothing term. For an energy to be graph-representable, the pairwise interaction potentials must be submodular [REF HERE], i.e. it

must adhere to the following constraint.

$$E^{i,j}(0,0) + E^{i,j}(1,1) \leq E^{i,j}(0,1) + E^{i,j}(1,0), \forall i < j. \tag{11}$$

It has been shown in [REF HERE] that Equation (8) is submodular and hence the optimal solution can be found via graph cuts. The data and regularisation energy respectively in Equation (10) is

$$E^i(x_i) = \lambda_1 |u(x,y) - c_1|^2 x_i + \lambda_2 |u(x,y) - c_2|^2 (1 - x_i) \tag{12}$$

$$E^{i,j}(x_i, x_j) = (x_i + x_j - 2x_i x_j) w_{ij} \tag{13}$$

IV. Chan-Vese Parameter Estimation for Graph-Cuts

In this section we introduce the proposed method for Chan-Vese parameter estimation for graph-cuts. Previous parameter estimation schemes focussed on a certain genre of images or image characteristics, and these resulted in a set of hard-coded parameter settings. These hard-coded parameters are not very useful in producing consistent results in the greater applications of image segmentation even within the fields for which they were optimised.

We devise a novel weighting scheme for the graph and propose a general parameter estimation technique in which the parameters adapt themselves to the image. We achieve this not by focusing on the parameters, but rather the relationship between the parameters. We then isolate these relationships in proxy relational parameters which we then tune for fluorescence images.

A. Proposed Technique

We first explain the method used to weight the graph. We begin by normalising the data and regularisation energies. The image pixel values are also normalised i.e. $p \in [0, 1]$, where p is the pixel value of the i-th pixel in the image. The weight of the edge connecting the source node to a pixel-node which corresponds to pixel i is given by $E^i(0)|_{i=p} = \lambda_0 |p - c_0|^2$. This is how far away the pixel is from the average foreground/object pixel intensity c_0. Similarly, the weight of the connection from the node to the sink is given by $E^i(1)|_{i=p} = \lambda_1 |p - c_1|^2$, i.e. how far away the pixel is from the average background pixel intensity c_1.

Whether a node is connected to the source or the sink after segmentation depends on its connections which are weighted by the previously defined energy functions. It behooves us then, to study the relationship between the energy functions. From Equation (8), we see that there are three tuneable parameters namely μ, λ_0 and λ_1. It is the relationship between these parameters that heavily influence the output. Firstly we will consider λ_0 and λ_1 whose relationship we simplify and explicitely formalise to

$$\lambda_0 = \alpha \lambda_1. \tag{14}$$

Forcing this relationship make further analysis simpler and more intuitive. An immediate constraint is $\alpha > 0$, since we require all data conenctions to be positive, i.e $E^i(0), E^i(1) \geq 0$.

We will now analyse the flow through a single node in the 8-connected graph, we use Figure 1 to facilitate our explanation. Two nodes are maximally connected if their corresponding pixel values are the same, i.e. there is no difference between them. Let the weight of the edge between two nodes whose pixels have the same intensity be μ. Hence, the maximum possible flow into or out of a node to its neighbours is

$$f_{max} = 4\mu + 4\frac{\mu}{\sqrt{2}} = \mu \left(2\sqrt{2} + 4\right). \tag{15}$$

We know that for a node p to belong to the source set, i.e. $p \in S$, the incoming flow from the source must completely saturate all outlets. This can be expressed as

$$E^i(0) > E^i(1) + \mu\left(2\sqrt{2}+4\right). \tag{16}$$

Similarly, to guarantee the node will be in the sink set, $p \in T$, we have

$$E^i(1) > E^i(0) + \mu\left(2\sqrt{2}+4\right). \tag{17}$$

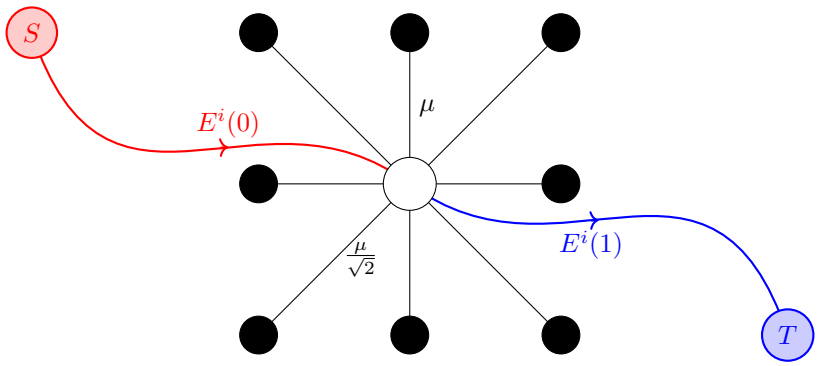

Fig. 1. Fully connected single node.

To aid in understanding the energies, we use Figure 2.

For quadratic energies with $0 < c_0 < c_1 < 1$, there is a point, between c_0 and c_1, where the incoming flow from the source completely saturates the sink with no excess remaining. This point, where the energies are equal, we call p_e, i.e. $E_0(p_e) = E_1(p_e)$. Taking into account the relation in Equation (14), this point of zero net flow is found to be

$$p_e = c_0 + \frac{c_1 - c_0}{\sqrt{\alpha}+1} \tag{18}$$

The point where the energies are equal, p_e, is shown in Figure 2.

We now shift our focus on the relationship between p_e and α. From Equation (18) we see that α is the only tuneable parameter. From this inverse relationship we note three major points. These are

$$\begin{aligned} \text{if } \alpha = 1, p_e &= \frac{c_0 + c_1}{2} && \text{(midpoint between } c_0 \text{ and } c_1) \\ \lim_{\alpha\to\infty} p_e &= c_0 && \text{(maximum } \alpha \text{ yields lower-bound on } p_e) \\ \lim_{\alpha\to 0} p_e &= c_1 && \text{(minimum } \alpha \text{ yields upper-bound on } p_e) \end{aligned}$$

This is relationship is shown graphically in Figure 3.

If we can make a good estimation for p_e, c_0 and c_1 for the segmentated image, then it can be shown that the corresponding α can be calculated as

$$\alpha = \left(\frac{c_1 - c_0}{p_e - c_0} - 1\right)^2 \tag{19}$$

When we calculated the intersection between the energies p_e, we ignored the other point that was out of the range $[c_0, c_1]$.Let this point be p_{e^*}. If this point is positive and $0 < p_{e^*} < c_0$ then we must ensure that at no point

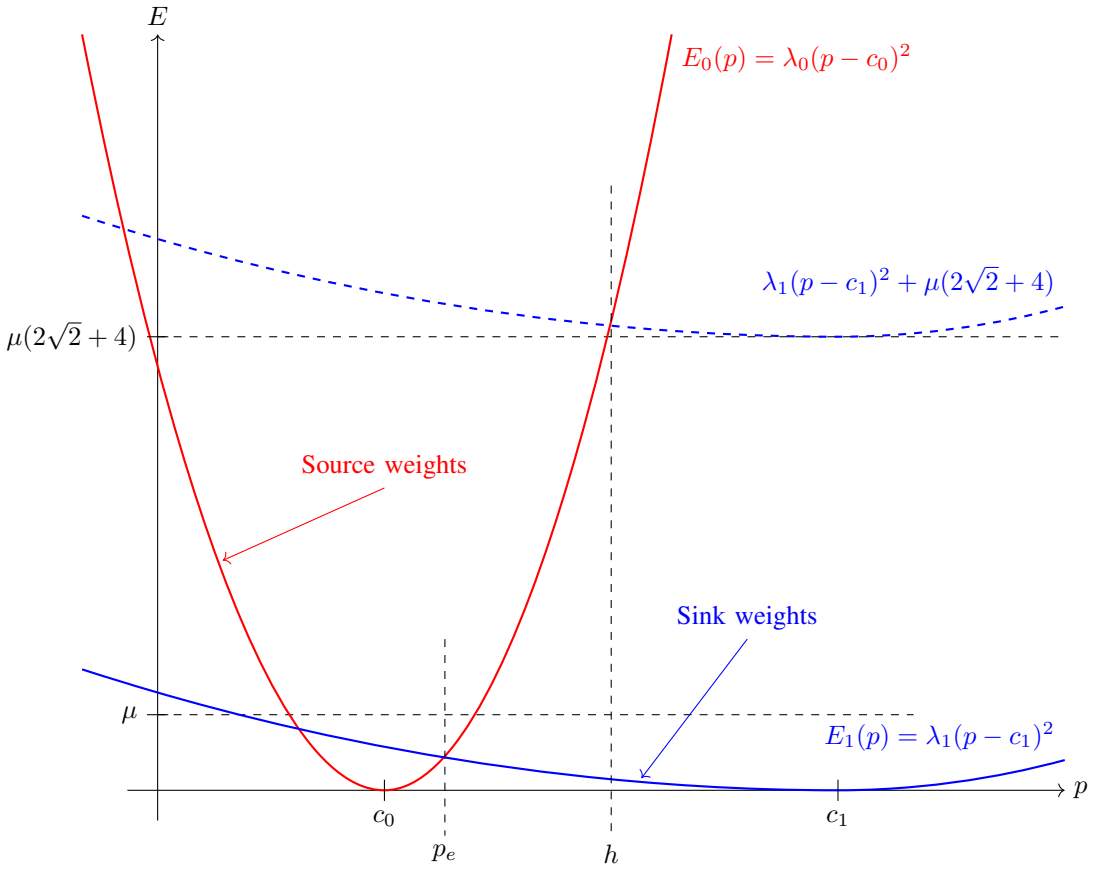

Fig. 2. Data energy functions plot.

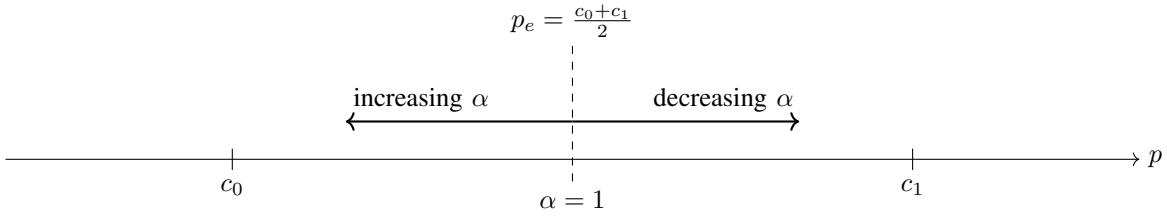

Fig. 3. Relationship between α and p_e.

within this range must the source flow saturate all outgoing edges. This forces a limit on how low μ can be. This is only of significant concern when $\alpha > 1$. We only need to concern ourselves with the point $p = 0$ as this is the point where the difference $E^i(0) - E^i(1)$ is the largest. Taking into account the relation in Equation (14), the lower-bound on μ can be shown to be

$$\mu > \frac{\lambda_1(\alpha c_0^2 - c_1^2)}{C} \tag{20}$$

We set $C = \left(2\sqrt{2} + 4\right)$ which is the sum of all the attenuating factors of the edges connected to a node.

From Equation (16) we can see that there is a point beyond which all nodes which correspond to pixel value

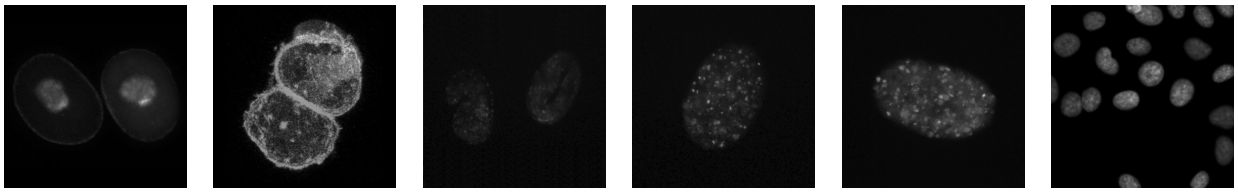

(a) Image 1 (b) Image 2 (c) Image 3 (d) Image 4 (e) Image 5 (f) Image 6

Fig. 4. Images from tuning set.

higher than that point will be saturated and have excess flow; this means that they will be in the source set. We will call this point the *saturation point* and denote it by h. This is shown in Figure 2. This point can be determined using

$$h = \frac{(\alpha c_0 - c_1) + \sqrt{\alpha(c_0 - c_1)^2 + \frac{C\mu}{\lambda_1}(\alpha - 1)}}{\alpha - 1} \tag{21}$$

This point is marked off in Figure 2.

Therefore, given good approximations for c_0, c_1, α, h and μ, we can calculate the appropriate value for λ_1. This can be shown to be

$$\lambda_1 = \frac{C\mu}{\alpha(h - c_0)^2 - (h - c_1)^2} \tag{22}$$

The parameter estimation is based on the assumption that sufficiently good approximations for c_0, c_1, p_e and h can be obtained. By sufficiently good we are referring to the closeness to the values these parameters would be for an ideal segmentation. From these approximations, we calculate α using Equation (19). The parameters μ and λ_1 are not separable, therefore we choose to set μ. We can then calculate λ_1 using Equation (22). Finally λ_0 can be calculated using Equation (14). In the next section we discuss how we make the guess for good approximations for the required parameters.

B. Tuning the Proxy Parameters

The properties of the images obtained in fluorescence microscopy imaging can be used to guide the parameter estimation process. We focus specifically on black background fluorescent images. Due to the fact that the predominant form of noise in the imaging system in Poisson distributed, we can further assume that the darker the background, the less noise that is present therein. The Poisson process also tells us that brighter regions exhibit a greater intensity variation due to the sampling process. Therefore, the curve for $E^i(1)$ is less convex than $E^i(0)$ as in Figure 2 and, resultantly, the value for p_e, in Figure 3, is shifted to the left. This places a new lower-bound on α for fluorescence images

$$\alpha \geq 1. \tag{23}$$

The tuning process we used is as follows: We manually segmented the fluorescent images in Figure 4. The segmentation results that were closest to the groundtruth were chosen and the corresponding proxy parameters were calculated for each image. The final setting for the proxy parameter was taken as the average value for each proxy parameter from all images.

Since the curves energy functions, $E^i(0)$ and $E^i(1)$, can be tuned relative to a fixed value for μ, which would not impact significantly on the range of possible solution sets, we set $\mu = 1$ in all our manual parameter tuning. We use a stopping criterion of $\epsilon = 1 \times 10^{-3}$. We compared the effect of using Otsu binarization, K-means ($k = 2$) and Expectation-Maximisation for Gaussian Mixture Modelling (EMGMM) with ($k = 2$) for generating the initial means, $c0$ and c_1. The values used for $\alpha \in [1, 10, 20, 30, 40, 45, 50]$ and the values used for $\lambda_1 \in [50, 100, 150, 200, 400, 800]$. The remaining parameters were calculated from μ, α and λ_1.

As final results we take the means of the final segmentation for the background and foreground regions. An acceptable solution was one that achieved at least 70% of the final means from the ground truth for each region. From the acceptable results, we calculate the values for p_e, Equation (18), and h, Equation (21). The means for each image can vary greatly. To put the values of p_e and h into a relative perspective, they are shown as a fraction of the distance between c_0 and c_1. Let $k_p \in (0, 1)$ be the fraction of the distance $p_e - c_0$ and $c_1 - c_0$ as illustrated in Figure 5. Let $k_h \in (k_h, 1)$ be the fraction of the distance $h - c_0$ and $c_1 - c_0$ as illustrated in Figure 6, we have $0 < k_p < k_h$.

Fig. 5. p_e as a fraction of the distance between c_0 and c_1.

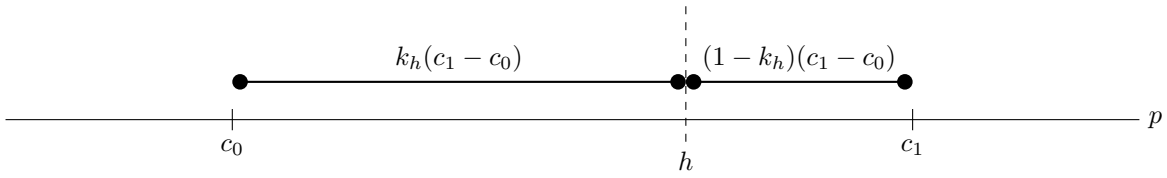

Fig. 6. h as a fraction of the distance between c_0 and c_1.

Upon comparing the initial means and final means for the acceptable segmentation results, it was noted the the values of the initial means are larger. This is due to over-segmentation produced by Otsu, K-means and EMGMM clustering. A naïve approach to shifting the initial means closer to the final means is to dilate the initial mask. This pushes the boundaries of the contour for the object to accept the lower intensity neighbouring pixels, as well as remove these relatively higher values from the background mask. If we are able to make a better guess to the initial means, then the fewer iterations are needed to converge within the stopping criterion.

To determine the optimal dilation size, we compare the difference of the mean values for each image, for the acceptable segmentation results only. We use an elliptical element for dilation and the size of the dilation ranged from $r \in [1, 2, 3, 5, 7, 9]$. A dilation size of 3 for a elliptical dilation element results in mean values that are closest to the average final means.

When defining the values for p_e and h implicitly and k_p and k_h respectively, we find the updated equation for determining α is simplified to

$$\alpha = \left(\frac{1-k_p}{k_p}\right)^2 \tag{24}$$

The weighting parameter λ_1 can be calculated as

$$\lambda_1 = \frac{C\mu}{(c_1-c_0)^2\left(\left(\frac{1-2k_p}{k_p^2}\right)k_h^2 + 2k_h - 1\right)} \tag{25}$$

For determining α we found the average of all k_p for all acceptable segmentations. This is calculated to be

$$k_p = 0.154494.$$

From this we can calculate the value for α immediately using Equation (24). This turns out to be

$$\alpha = 29.9509. \tag{26}$$

Similarly, to determine h we find the average of all k_h for all acceptable segmentations. This is calculated to be

$$k_h = 0.412737.$$

An appropriate value for λ_1 depends on c_0 and c_1, as can be seen in Equation (25), which can only be determined after the inital means are generated.

V. Experimental Results

We compare our results to two previously published parameter settings. The first is the parameter settings used El Zehiry *et al.* [**?**], which is where the Chan-Vese Graph Cut technique was first published. Their results showed excellent segmentation output on synthetic images and mammography images with very high robustness against noise. They do not specify the noise type. The second parameter setting which we compete against is presented by Masaka *et al.* [**?**]. Their parameter setting was based on a time-lapse series of fluorescence images. Their scheme is a hybrid of algorithms designed to segment whole fluorescent cells; however, we use the parameter setting they have presented for segmentation only. Their parameter setting was obtained by minimising the Jaccard coefficient over the time-lapse series.

To generate the initial means we used the EMGMM with $k = 2$ which was followed by an elliptical dilation of size 3. The results of all segmentation scheme are shown from Figure 7 to Figure 21.

In Table I we compare the accuracy and MCC of each segmented result for each scheme. Accuracy is the fraction of the pixels that are correctly classified from among all pixels. MCC is the *Matthews Correlation Coefficient* and is a more accurate measure of accuracy when comparing classes whose sizes differ greatly. We used an 8-connected graph for all methods. The overall segmenation efficiency for the entire test set of 25 images is shown in Table II.

TABLE I: Segmentation Efficiency.

Image	El-Zehiry *et. al*		Masaka *et. al*		Proposed	
	Accuracy	MCC	Accuracy	MCC	Accuracy	MCC

1	0.770111	0.626140	0.967117	0.934010	0.959427	0.919468
2	0.747253	0.416180	0.335449	-0.008374	0.862671	0.748686
3	0.912262	0.811918	0.851883	0.739708	0.916992	0.842769
4	0.515686	0.300907	0.603195	0.028915	0.966156	0.931253
5	0.886490	0.589732	0.938583	0.834732	0.990768	0.970635
6	0.806732	0.519903	0.309845	0.060018	0.905685	0.808358
7	0.962357	0.507270	0.098129	0.051537	0.990158	0.911074
8	0.888229	0.452365	0.150055	0.020336	0.915009	0.733933
9	0.595612	0.384991	0.567032	NaN	0.960739	0.922580
10	0.852585	0.559970	0.570099	0.393942	0.975266	0.933388
11	0.914856	0.719637	0.679703	0.479944	0.966690	0.904878
12	0.913818	0.678954	0.181793	0.035231	0.967438	0.885155
13	0.703156	0.469557	0.449310	NaN	0.981735	0.963345
14	0.921356	0.562635	0.136047	0.047223	0.882690	0.661018
15	0.573715	0.296608	0.511276	NaN	0.959915	0.920148

TABLE II: Overall Segmentation Efficiency.

Method	Accuracy	
	Mean	Std. Dev
El-Zehiry *et al.*	0.805732	0.151199
Maska *et al.*	0.547369	0.321099
Proposed	0.935329	0.064493

The general parameter settings by El-Zehiry *et al.* clearly outperform by the parameter settings presented by Masaka *et al.* by a 25.8363% difference in accuracy. However, the proposed method boasts an increase of 12.9597% above El-Zehiry's parameter settings. The proposed method is also much more stable over a greater variety of fluorescence images, as can be seen by the standard deviation of accuracy shown in Table II.

VI. Conclusion

Fluorescence images are hugely diverse; even so of the images within the fields of cellular biology and medicine. The design of a general and automatic segmentation method is not a trivial exercise; and, it is much needed.

We have presented a novel parameter estimation technique which is able to tune the parameters of the graph-cut application of the Chan-Vese segmentation method, to the specific image. This is a huge contrast in comparison to the fixed parameter settings proposed by El-Zehiry *et al.* and Masaka *et al.* Our method, does however, rely on the strong assumption that the initial means obtained from the initial unsupervised segmentation scheme is relatively close to the final means. Fortunately though, in the domain of biological and medical fluorescence images, the unsupervised segmentation results obtained from an Otsu, K-means or EMGMM clustering is close enough to

outperform the competitor parameter settings. We have shown that an EMGMM clustering and a dilation of 3 pixels, with an elliptical dilation element, provides the best approximation to the final means which results in an average of 93.5329% classification accuracy. Given the diversity of fluorescence images in the test set, this is a very pleasing result, especially when compared to the competitor parameter settings by El-Zehiry *et al.* which showed an average of 80.5732% and Masaka *et al.* which showed an average of 54.7369%.

Once the initial means have been obtained, the parameters are adapted to the image by direct calculation by means of the *relationship variables and formulae*. These relationship variables and formulae encode the important relation of the parameters with each other. This allows the ability to adapt the parameter settings according to the properties of the image. These resutling parameters only allow high segmentation accuracy if the image has the properties that are encoded in the relationship variables and formulae.

The relationship formulae only take into account the infomation from the intensity of the image. Other infomation, such as texture, can be incorporated into the formulae as well. This will include adapting the graph to hold this infomation so that it can be accounted for in the energy function.

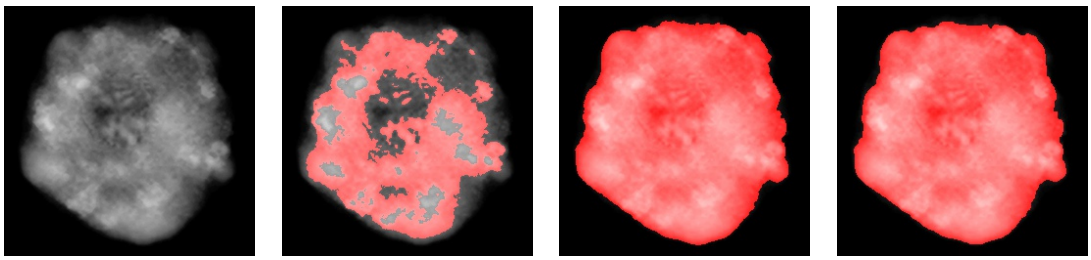

(a) Original. (b) El-Zehiry *et al*. (c) Masaka *et al*. (d) Proposed. $\lambda_1 = 8.17148$.

Fig. 7. Image 1 from test set segmentation results.

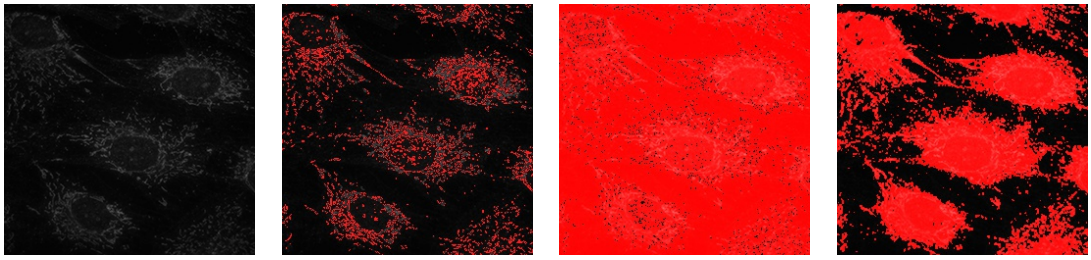

(a) Original. (b) El-Zehiry *et al*. (c) Masaka *et al*. (d) Proposed. $\lambda_1 = 606.199$.

Fig. 8. Image 2 from test set segmentation results.

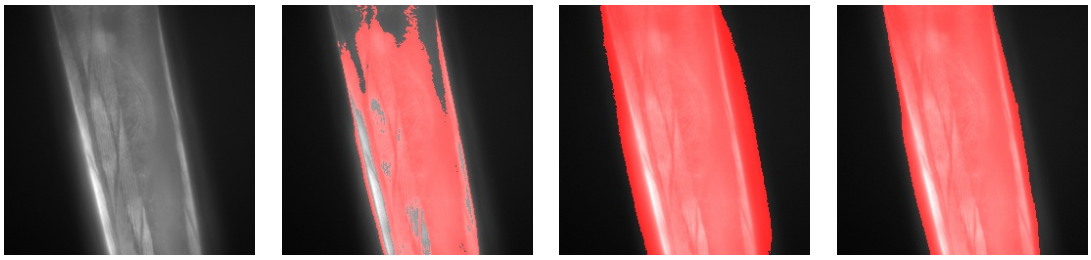

(a) Original. (b) El-Zehiry *et al*. (c) Masaka *et al*. (d) Proposed. $\lambda_1 = 11.2011$.

Fig. 9. Image 3 from test set segmentation results.

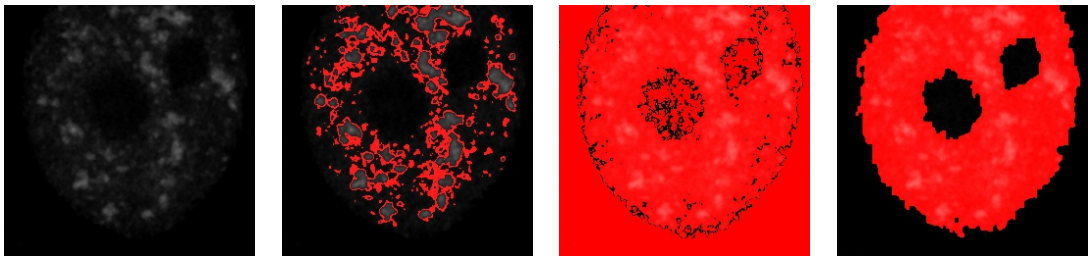

(a) Original. (b) El-Zehiry *et al*. (c) Masaka *et al*. (d) Proposed. $\lambda_1 = 161.108$.

Fig. 10. Image 4 from test set segmentation results.

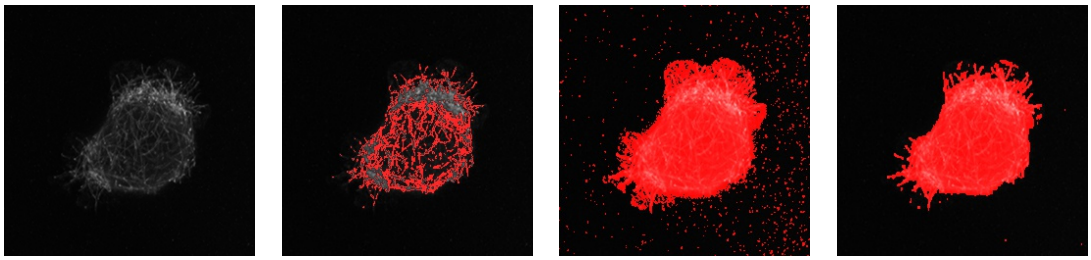

(a) Original. (b) El-Zehiry *et al*. (c) Masaka *et al*. (d) Proposed. $\lambda_1 = 146.629$.

Fig. 11. Image 5 from test set segmentation results.

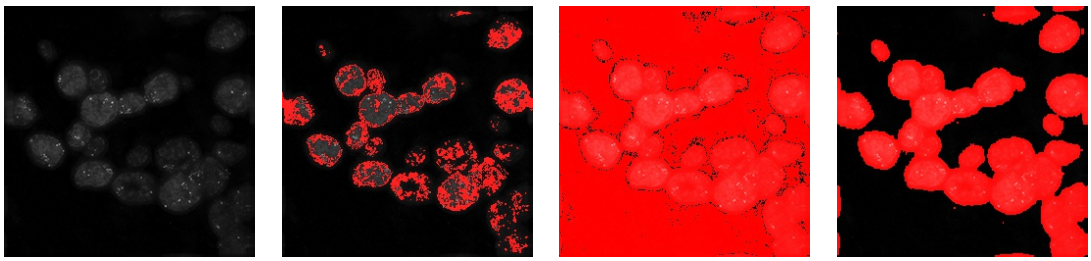

(a) Original. (b) El-Zehiry *et al*. (c) Masaka *et al*. (d) Proposed. $\lambda_1 = 160.407$.

Fig. 12. Image 6 from test set segmentation results.

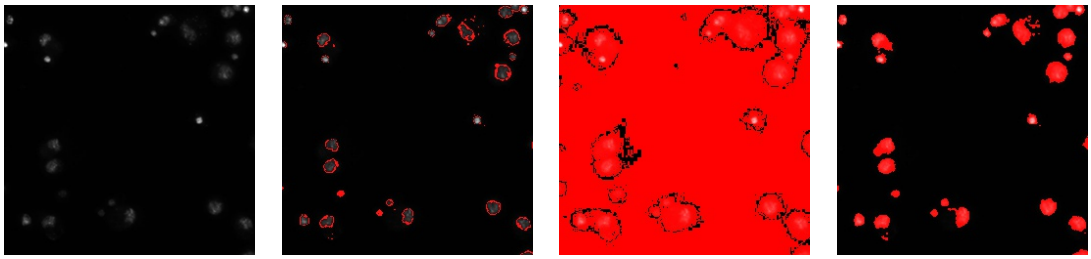

(a) Original. (b) El-Zehiry *et al*. (c) Masaka *et al*. (d) Proposed. $\lambda_1 = 860.426$.

Fig. 13. Image 7 from test set segmentation results.

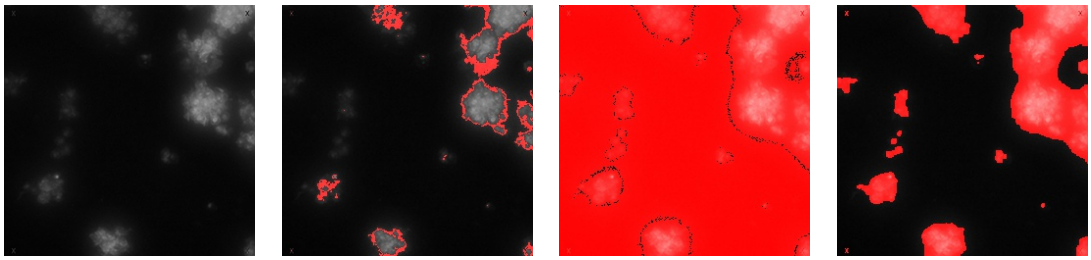

(a) Original. (b) El-Zehiry *et al*. (c) Masaka *et al*. (d) Proposed. $\lambda_1 = 43.33$.

Fig. 14. Image 8 from test set segmentation results.

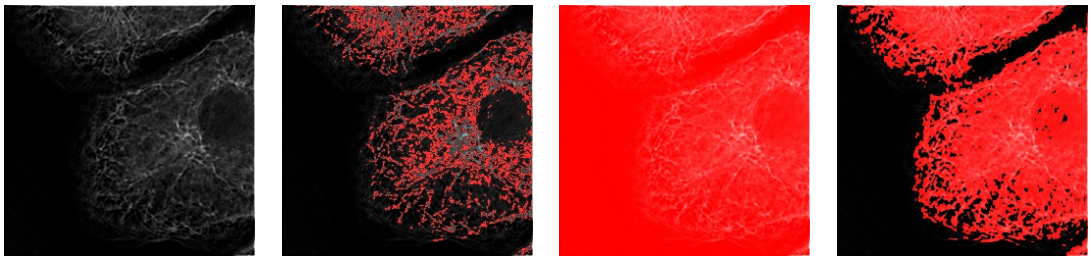

(a) Original. (b) El-Zehiry *et al*. (c) Masaka *et al*. (d) Proposed. $\lambda_1 = 85.0788$.

Fig. 15. Image 9 from test set segmentation results.

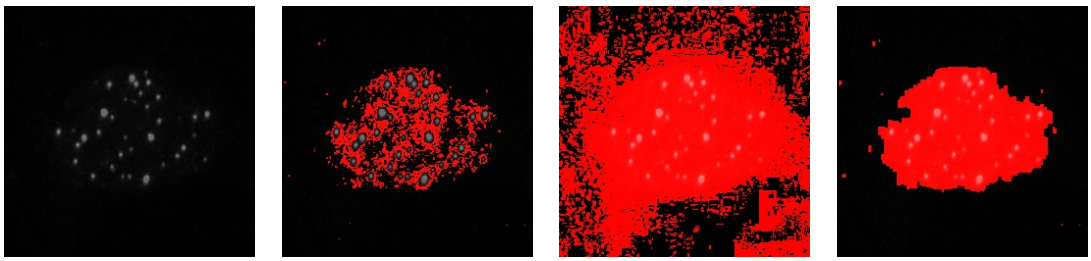

(a) Original. (b) El-Zehiry *et al*. (c) Masaka *et al*. (d) Proposed. $\lambda_1 = 309.766$.

Fig. 16. Image 10 from test set segmentation results.

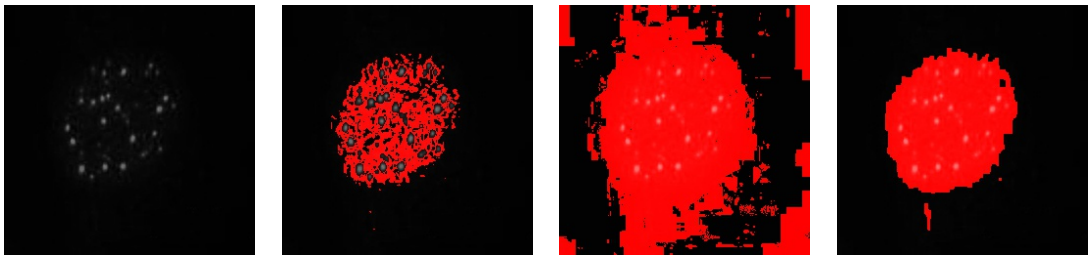

(a) Original. (b) El-Zehiry *et al*. (c) Masaka *et al*. (d) Proposed. $\lambda_1 = 359.465$.

Fig. 17. Image 11 from test set segmentation results.

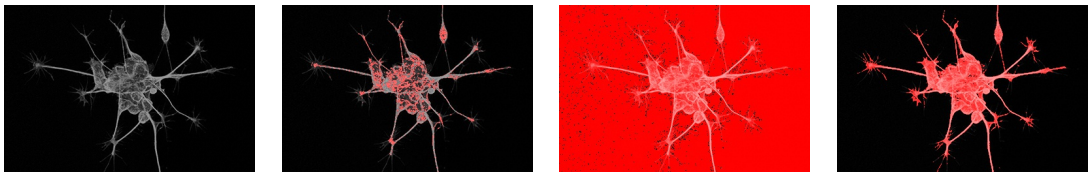

(a) Original. (b) El-Zehiry *et al*. (c) Masaka *et al*. (d) Proposed. $\lambda_1 = 359.465$.

Fig. 18. Image 12 from test set segmentation results.

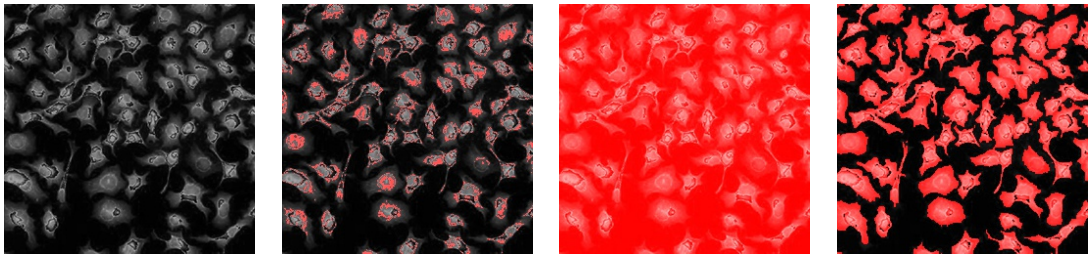

(a) Original. (b) El-Zehiry *et al*. (c) Masaka *et al*. (d) Proposed. $\lambda_1 = 38.837$.

Fig. 19. Image 13 from test set segmentation results.

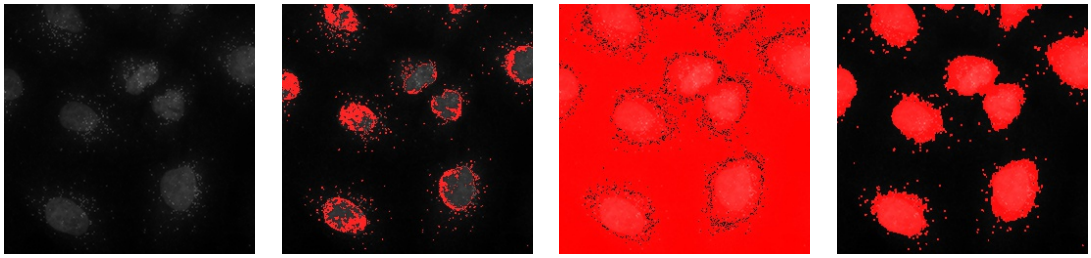

(a) Original. (b) El-Zehiry *et al*. (c) Masaka *et al*. (d) Proposed. $\lambda_1 = 249.515$.

Fig. 20. Image 13 from test set segmentation results.

4

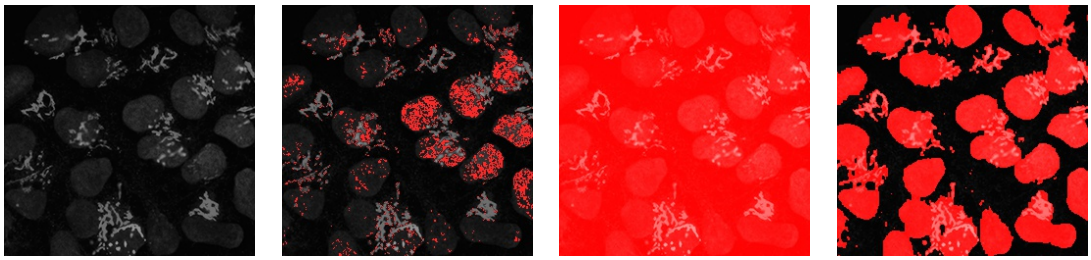

(a) Original. (b) El-Zehiry *et al*. (c) Masaka *et al*. (d) Proposed. $\lambda_1 = 118.726$.

Fig. 21. Image 15 from test set segmentation results.